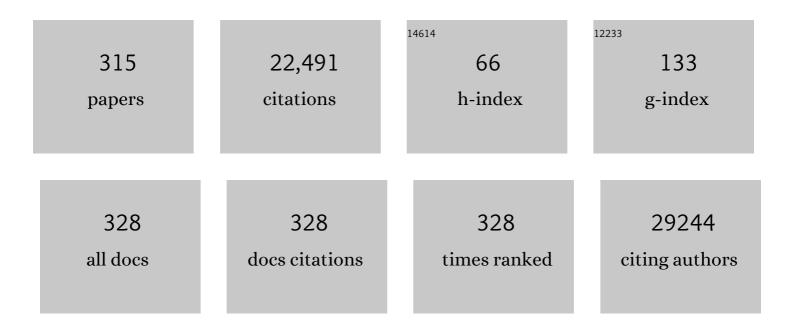
List of Publications by Year in descending order

Source: https://exaly.com/author-pdf/276681/publications.pdf Version: 2024-02-01



#	Article	IF	CITATIONS
1	Inactivation of the ferroptosis regulator Gpx4 triggers acute renal failure in mice. Nature Cell Biology, 2014, 16, 1180-1191.	4.6	2,241
2	ACSL4 dictates ferroptosis sensitivity by shaping cellular lipid composition. Nature Chemical Biology, 2017, 13, 91-98.	3.9	2,069
3	Monocytes, neutrophils, and platelets cooperate to initiate and propagate venous thrombosis in mice in vivo. Journal of Experimental Medicine, 2012, 209, 819-835.	4.2	1,441
4	Selenium Utilization by GPX4 Is Required to Prevent Hydroperoxide-Induced Ferroptosis. Cell, 2018, 172, 409-422.e21.	13.5	920
5	The target landscape of clinical kinase drugs. Science, 2017, 358, .	6.0	609
6	Quantitative Gene Expression Analysis in Microdissected Archival Formalin-Fixed and Paraffin-Embedded Tumor Tissue. American Journal of Pathology, 2001, 158, 419-429.	1.9	461
7	HER2 diagnostics in gastric cancer—guideline validation and development of standardized immunohistochemical testing. Virchows Archiv Fur Pathologische Anatomie Und Physiologie Und Fur Klinische Medizin, 2010, 457, 299-307.	1.4	431
8	MALDI Imaging mass spectrometry: current frontiers and perspectives in pathology research and practice. Laboratory Investigation, 2015, 95, 422-431.	1.7	334
9	MALDI imaging mass spectrometry for direct tissue analysis: a new frontier for molecular histology. Histochemistry and Cell Biology, 2008, 130, 421-34.	0.8	310
10	Classification of HER2 Receptor Status in Breast Cancer Tissues by MALDI Imaging Mass Spectrometry. Journal of Proteome Research, 2010, 9, 1854-1863.	1.8	256
11	Mitochondrial glutathione peroxidase 4 disruption causes male infertility. FASEB Journal, 2009, 23, 3233-3242.	0.2	251
12	Disulfide HMGB1 derived from platelets coordinates venous thrombosis in mice. Blood, 2016, 128, 2435-2449.	0.6	219
13	Normalization in MALDI-TOF imaging datasets of proteins: practical considerations. Analytical and Bioanalytical Chemistry, 2011, 401, 167-181.	1.9	190
14	High-mass-resolution MALDI mass spectrometry imaging of metabolites from formalin-fixed paraffin-embedded tissue. Nature Protocols, 2016, 11, 1428-1443.	5.5	190
15	Steroid metabolome analysis reveals prevalent glucocorticoid excess in primary aldosteronism. JCI Insight, 2017, 2, .	2.3	187
16	Aurora Kinase A Messenger RNA Overexpression Is Correlated with Tumor Progression and Shortened Survival in Head and Neck Squamous Cell Carcinoma. Clinical Cancer Research, 2006, 12, 5136-5141.	3.2	176
17	Inflammation and mitochondrial fatty acid β-oxidation link obesity to early tumor promotion. Proceedings of the National Academy of Sciences of the United States of America, 2009, 106, 3354-3359.	3.3	174
18	Distribution Pattern of Inhaled Ultrafine Gold Particles in the Rat Lung. Inhalation Toxicology, 2006, 18, 733-740.	0.8	173

#	Article	IF	CITATIONS
19	Platelets contribute to postnatal occlusion of the ductus arteriosus. Nature Medicine, 2010, 16, 75-82.	15.2	158
20	Data-driven identification of prognostic tumor subpopulations using spatially mapped t-SNE of mass spectrometry imaging data. Proceedings of the National Academy of Sciences of the United States of America, 2016, 113, 12244-12249.	3.3	154
21	Typical and Atypical Carcinoid Tumors of the Lung Are Characterized by 11q Deletions as Detected by Comparative Genomic Hybridization. American Journal of Pathology, 1998, 153, 1089-1098.	1.9	151
22	Evaluation of α <sub>v</sub> β <sub>3</sub> Integrin-Targeted Positron Emission Tomography Tracer <sup>18</sup> F-Galacto-RGD for Imaging of Vascular Inflammation in Atherosclerotic Mice. Circulation: Cardiovascular Imaging, 2009, 2, 331-338.	1.3	145
23	Chromosomal Imbalances in Barrett's Adenocarcinoma and the Metaplasia-Dysplasia-Carcinoma Sequence. American Journal of Pathology, 2000, 156, 555-566.	1.9	144
24	Extracellular Matrix Metalloproteinase Inducer (CD147) Is a Novel Receptor on Platelets, Activates Platelets, and Augments Nuclear Factor κB–Dependent Inflammation in Monocytes. Circulation Research, 2008, 102, 302-309.	2.0	138
25	Impaired Autophagy Induces Chronic Atrophic Pancreatitis in Mice via Sex- and Nutrition-Dependent Processes. Gastroenterology, 2015, 148, 626-638.e17.	0.6	130
26	Patch repair of deep wounds by mobilized fascia. Nature, 2019, 576, 287-292.	13.7	129
27	Bioengineered bacterial vesicles as biological nano-heaters for optoacoustic imaging. Nature Communications, 2019, 10, 1114.	5.8	128
28	MALDI Imaging Identifies Prognostic Seven-Protein Signature of Novel Tissue Markers in Intestinal-Type Gastric Cancer. American Journal of Pathology, 2011, 179, 2720-2729.	1.9	127
29	Combined Deficiency in Glutathione Peroxidase 4 and Vitamin E Causes Multiorgan Thrombus Formation and Early Death in Mice. Circulation Research, 2013, 113, 408-417.	2.0	127
30	Increased Extracellular Vesicles Mediate WNT5A Signaling in Idiopathic Pulmonary Fibrosis. American Journal of Respiratory and Critical Care Medicine, 2018, 198, 1527-1538.	2.5	127
31	A Novel Antifibrotic Mechanism of Nintedanib and Pirfenidone. Inhibition of Collagen Fibril Assembly. American Journal of Respiratory Cell and Molecular Biology, 2017, 57, 77-90.	1.4	125
32	Tumor Classification of Six Common Cancer Types Based on Proteomic Profiling by MALDI Imaging. Journal of Proteome Research, 2012, 11, 1996-2003.	1.8	123
33	Highâ€resolution MALDIâ€FTâ€ICR MS imaging for the analysis of metabolites from formalinâ€fixed, paraffinâ€embedded clinical tissue samples. Journal of Pathology, 2015, 237, 123-132.	2.1	123
34	Intratumoral Heterogeneity in Breast Carcinoma Revealed by Laser-Microdissection and Comparative Genomic Hybridization. Cancer Genetics and Cytogenetics, 1999, 110, 94-102.	1.0	122
35	Exploring Three-Dimensional Matrix-Assisted Laser Desorption/Ionization Imaging Mass Spectrometry Data: Three-Dimensional Spatial Segmentation of Mouse Kidney. Analytical Chemistry, 2012, 84, 6079-6087.	3.2	122
36	<i>De novo</i> discovery of phenotypic intratumour heterogeneity using imaging mass spectrometry. Journal of Pathology, 2015, 235, 3-13.	2.1	116

#	Article	IF	CITATIONS
37	Molecular Analysis of HER2 Signaling in Human Breast Cancer by Functional Protein Pathway Activation Mapping. Clinical Cancer Research, 2012, 18, 6426-6435.	3.2	110
38	MALDI imaging mass spectrometry for direct tissue analysis: technological advancements and recent applications. Histochemistry and Cell Biology, 2011, 136, 227-244.	0.8	108
39	Tissueâ€based proteomics reveals FXYD3, S100A11 and GSTM3 as novel markers for regional lymph node metastasis in colon cancer. Journal of Pathology, 2012, 228, 459-470.	2.1	107
40	p62 Links β-adrenergic input to mitochondrial function and thermogenesis. Journal of Clinical Investigation, 2013, 123, 469-478.	3.9	107
41	Genomic Alterations and Allelic Imbalances Are Strong Prognostic Predictors in Osteosarcoma. Clinical Cancer Research, 2010, 16, 4256-4267.	3.2	101
42	Mitochondrial Dysfunction and Decrease in Body Weight of a Transgenic Knock-in Mouse Model for TDP-43. Journal of Biological Chemistry, 2014, 289, 10769-10784.	1.6	100
43	Histopathological Classification of Nonneoplastic and Neoplastic Gastrointestinal Submucosal Lesions. Endoscopy, 2005, 37, 630-634.	1.0	99
44	Extensive ductal carcinomaln situ with small foci of invasive ductal carcinoma: Evidence of genetic resemblance by CGH. International Journal of Cancer, 2000, 85, 82-86.	2.3	97
45	Imaging of pH in vivo using hyperpolarized 13C-labelled zymonic acid. Nature Communications, 2017, 8, 15126.	5.8	94
46	STAT3 mRNA and protein expression in colorectal cancer: effects on STAT3-inducible targets linked to cell survival and proliferation. Journal of Clinical Pathology, 2006, 60, 173-179.	1.0	92
47	MALDI imaging mass spectrometry reveals COX7A2, TAGLN2 and S100-A10 as novel prognostic markers in Barrett's adenocarcinoma. Journal of Proteomics, 2012, 75, 4693-4704.	1.2	90
48	N-acyl Taurines and Acylcarnitines Cause an Imbalance in Insulin Synthesis and Secretion Provoking β Cell Dysfunction in Type 2 Diabetes. Cell Metabolism, 2017, 25, 1334-1347.e4.	7.2	87
49	Atlas of exercise metabolism reveals time-dependent signatures of metabolic homeostasis. Cell Metabolism, 2022, 34, 329-345.e8.	7.2	86
50	Immunocytochemical and Ultrastructural Evidence of Glial Cells and Hyalocytes in Internal Limiting Membrane Specimens of Idiopathic Macular Holes. , 2011, 52, 7822.		84
51	Mutations in the mitochondrial thioredoxin reductase gene TXNRD2 cause dilated cardiomyopathy. European Heart Journal, 2011, 32, 1121-1133.	1.0	84
52	Distribution and quantification of irinotecan and its active metabolite SN-38 in colon cancer murine model systems using MALDI MSI. Analytical and Bioanalytical Chemistry, 2015, 407, 2107-2116.	1.9	84
53	Proton Minibeam Radiation Therapy Reduces Side Effects in an InÂVivo Mouse Ear Model. International Journal of Radiation Oncology Biology Physics, 2016, 95, 234-241.	0.4	82
54	Gene-by-Sex Interactions in Mitochondrial Functions and Cardio-Metabolic Traits. Cell Metabolism, 2019, 29, 932-949.e4.	7.2	79

#	Article	IF	CITATIONS
55	Cadherin-2 Controls Directional Chain Migration of Cerebellar Granule Neurons. PLoS Biology, 2009, 7, e1000240.	2.6	78
56	MALDI imaging mass spectrometry in cancer research: Combining proteomic profiling and histological evaluation. Clinical Biochemistry, 2013, 46, 539-545.	0.8	77
57	PTK (protein tyrosine kinase)-6 and HER2 and 4, but not HER1 and 3 predict long-term survival in breast carcinomas. British Journal of Cancer, 2007, 96, 801-807.	2.9	75
58	The redox environment triggers conformational changes and aggregation of hIAPP in Type II Diabetes. Scientific Reports, 2017, 7, 44041.	1.6	75
59	Efficient Isolation of Pure and Functional Mitochondria from Mouse Tissues Using Automated Tissue Disruption and Enrichment with Anti-TOM22 Magnetic Beads. PLoS ONE, 2013, 8, e82392.	1.1	74
60	Enhanced Activation of Epidermal Growth Factor Receptor Caused by Tumor-Derived E-Cadherin Mutations. Cancer Research, 2008, 68, 707-714.	0.4	72
61	Multicenter Matrix-Assisted Laser Desorption/Ionization Mass Spectrometry Imaging (MALDI MSI) Identifies Proteomic Differences in Breast-Cancer-Associated Stroma. Journal of Proteome Research, 2014, 13, 4730-4738.	1.8	72
62	Genetic heterogeneity in a prostatic carcinoma and associated prostatic intraepithelial neoplasia as demonstrated by combined use of laser-microdissection, degenerate oligonucleotide primed PCR and comparative genomic hybridization. Virchows Archiv Fur Pathologische Anatomie Und Physiologie Und Fur Klinische Medizin, 1998, 433, 297-304.	1.4	71
63	Combined analysis of Rac1, IQGAP1, Tiam1 and E-cadherin expression in gastric cancer. Modern Pathology, 2008, 21, 544-552.	2.9	71
64	Classification of HER2/neu Status in Gastric Cancer Using a Breast-Cancer Derived Proteome Classifier. Journal of Proteome Research, 2010, 9, 6317-6322.	1.8	71
65	Clinical response to chemotherapy in oesophageal adenocarcinoma patients is linked to defects in mitochondria. Journal of Pathology, 2013, 230, 410-419.	2.1	71
66	Calcineurin Links Mitochondrial Elongation with Energy Metabolism. Cell Metabolism, 2015, 22, 838-850.	7.2	71
67	Accumulation of Chromosomal Imbalances From Intraductal Proliferative Lesions to Adjacent In Situ and Invasive Ductal Breast Cancer. Diagnostic Molecular Pathology, 2000, 9, 14-19.	2.1	71
68	Comprehensive Identification of Proteins from MALDI Imaging. Molecular and Cellular Proteomics, 2013, 12, 2901-2910.	2.5	69
69	Expression of a Catalytically Inactive Mutant Form of Glutathione Peroxidase 4 (Gpx4) Confers a Dominant-negative Effect in Male Fertility. Journal of Biological Chemistry, 2015, 290, 14668-14678.	1.6	69
70	Revisiting Rat Spermatogenesis with MALDI Imaging at 20-μm Resolution. Molecular and Cellular Proteomics, 2011, 10, M110.005991.	2.5	68
71	Proteomic Analysis of PAXgene-Fixed Tissues. Journal of Proteome Research, 2010, 9, 5188-5196.	1.8	67
72	Opposing role of Notch1 and Notch2 in a KrasG12D-driven murine non-small cell lung cancer model. Oncogene, 2015, 34, 578-588.	2.6	67

5

#	Article	IF	CITATIONS
73	A Five-MicroRNA Signature Predicts Survival and Disease Control of Patients with Head and Neck Cancer Negative for HPV Infection. Clinical Cancer Research, 2019, 25, 1505-1516.	3.2	67
74	Effects of neoadjuvant radio-chemotherapy on 18F-FDG-PET in esophageal carcinoma. European Journal of Surgical Oncology, 2004, 30, 544-550.	0.5	65
75	Quantitative Chemical Proteomics Reveals New Potential Drug Targets in Head and Neck Cancer. Molecular and Cellular Proteomics, 2011, 10, M111.011635.	2.5	65
76	Fluorescent blood–brain barrier tracing shows intact leptin transport in obese mice. International Journal of Obesity, 2019, 43, 1305-1318.	1.6	64
77	Predictive Value of Aurora-A/STK15 Expression for Late Stage Epithelial Ovarian Cancer Patients Treated by Adjuvant Chemotherapy. Clinical Cancer Research, 2007, 13, 4083-4091.	3.2	63
78	Cytopathicity of <i>Chlamydia</i> is largely reproduced by expression of a single chlamydial protease. Journal of Cell Biology, 2008, 182, 117-127.	2.3	63
79	Qualitative and quantitative mass spectrometry imaging of drugs and metabolites in tissue at therapeutic levels. Histochemistry and Cell Biology, 2013, 140, 93-104.	0.8	63
80	Progressive stages of mitochondrial destruction caused by cell toxic bile salts. Biochimica Et Biophysica Acta - Biomembranes, 2013, 1828, 2121-2133.	1.4	62
81	Chromosomal changes during development and progression of prostate adenocarcinomas. British Journal of Cancer, 2001, 84, 202-208.	2.9	61
82	Multispectral optoacoustic tomography of myocardial infarction. Photoacoustics, 2013, 1, 3-8.	4.4	61
83	Stabilization and structural analysis of a membrane-associated hIAPP aggregation intermediate. ELife, 2017, 6, .	2.8	61
84	Her-2/neu Gene Amplification, Elevated mRNA Expression, and Protein Overexpression in the Metaplasia-Dysplasia-Adenocarcinoma Sequence of Barrett's Esophagus. Laboratory Investigation, 2001, 81, 791-801.	1.7	59
85	Biomarker analysis of cetuximab plus oxaliplatin/leucovorin/5-fluorouracil in first-line metastatic gastric and oesophago-gastric junction cancer: results from a phase II trial of the Arbeitsgemeinschaft Internistische Onkologie (AIO). BMC Cancer, 2011, 11, 509.	1.1	58
86	MRI-compatible pipeline for three-dimensional MALDI imaging mass spectrometry using PAXgene fixation. Journal of Proteomics, 2013, 90, 52-60.	1.2	58
87	Array-based comparative genomic hybridization for the detection of DNA sequence copy number changes in Barrett's adenocarcinoma. Journal of Pathology, 2004, 203, 780-788.	2.1	56
88	S100-A10, thioredoxin, and S100-A6 as biomarkers of papillary thyroid carcinoma with lymph node metastasis identified by MALDI Imaging. Journal of Molecular Medicine, 2012, 90, 163-174.	1.7	56
89	MiR-221/-222 differentiate prognostic groups in advanced breast cancers and influence cell invasion. British Journal of Cancer, 2013, 109, 2714-2723.	2.9	54
90	Heart‧pecific Knockout of the Mitochondrial Thioredoxin Reductase ( <i>Txnrd2</i> ) Induces Metabolic and Contractile Dysfunction in the Aging Myocardium. Journal of the American Heart Association, 2015, 4, .	1.6	54

#	Article	IF	CITATIONS
91	HER2 Expression, Test Deviations, and Their Impact on Survival in Metastatic Gastric Cancer: Results From the Prospective Multicenter VARIANZ Study. Journal of Clinical Oncology, 2021, 39, 1468-1478.	0.8	54
92	TO-PRO-3 is an optimal fluorescent dye for nuclear counterstaining in dual-colour FISH on paraffin sections. Histochemistry and Cell Biology, 2001, 115, 293-299.	0.8	53
93	Differential KIT expression in histological subtypes of adenoid cystic carcinoma (ACC) of the salivary gland. Oral Oncology, 2005, 41, 934-939.	0.8	53
94	Benchmark datasets for 3D MALDI- and DESI-imaging mass spectrometry. GigaScience, 2015, 4, 20.	3.3	53
95	MALDI Imaging Mass Spectrometry for In Situ Proteomic Analysis of Preneoplastic Lesions in Pancreatic Cancer. PLoS ONE, 2012, 7, e39424.	1.1	52
96	Significance of HER2 Low-Level Copy Gain in Barrett's Cancer: Implications for Fluorescence In situ Hybridization Testing in Tissues. Clinical Cancer Research, 2007, 13, 5115-5123.	3.2	51
97	High number of CD45RO+ tumor infiltrating lymphocytes is an independent prognostic factor in non-metastasized (stage I-IIA) esophageal adenocarcinoma. BMC Cancer, 2010, 10, 608.	1.1	51
98	Discussion point: reporting guidelines for mass spectrometry imaging. Analytical and Bioanalytical Chemistry, 2015, 407, 2035-2045.	1.9	51
99	Image analysis of immunohistochemistry is superior to visual scoring as shown for patient outcome of esophageal adenocarcinoma. Histochemistry and Cell Biology, 2015, 143, 1-9.	0.8	50
100	Deep tissue imaging: a review from a preclinical cancer research perspective. Histochemistry and Cell Biology, 2016, 146, 781-806.	0.8	50
101	Levels of the Autophagy-Related 5 Protein Affect Progression and Metastasis of Pancreatic Tumors in Mice. Gastroenterology, 2019, 156, 203-217.e20.	0.6	50
102	The Intratumoral Heterogeneity Reflects the Intertumoral Subtypes of Glioblastoma Multiforme: A Regional Immunohistochemistry Analysis. Frontiers in Oncology, 2020, 10, 494.	1.3	50
103	A Fibrin Glue Composition as Carrier for Nucleic Acid Vectors. Pharmaceutical Research, 2008, 25, 2946-2962.	1.7	49
104	Tissue microdissection techniques in quantitative genome and gene expression analyses. Histochemistry and Cell Biology, 2001, 115, 269-276.	0.8	48
105	Approaching MALDI molecular imaging for clinical proteomic research: current state and fields of application. Expert Review of Proteomics, 2010, 7, 927-941.	1.3	47
106	Morphometric Cell Classification for Singleâ€Cell MALDIâ€Mass Spectrometry Imaging. Angewandte Chemie - International Edition, 2020, 59, 17447-17450.	7.2	47
107	Diet-induced alteration of intestinal stem cell function underlies obesity and prediabetes in mice. Nature Metabolism, 2021, 3, 1202-1216.	5.1	47
108	Flattop regulates basal body docking and positioning in mono- and multiciliated cells. ELife, 2014, 3, .	2.8	47

#	Article	IF	CITATIONS
109	Prognostic value of protein tyrosine kinase 6 (PTK6) for long-term survival of breast cancer patients. British Journal of Cancer, 2008, 99, 1089-1095.	2.9	45
110	Clinical Significance of the Costimulatory Molecule B7-H1 in Barrett Carcinoma. Annals of Thoracic Surgery, 2011, 91, 1025-1031.	0.7	45
111	MALDI-MS tissue imaging identification of biliverdin reductase B overexpression in prostate cancer. Journal of Proteomics, 2013, 91, 500-514.	1.2	45
112	Assessment of ErbB2 (Her2) in oesophageal adenocarcinomas: summary of a revised immunohistochemical evaluation system, bright field double in situ hybridisation and fluorescence in situ hybridisation. Modern Pathology, 2011, 24, 908-916.	2.9	44
113	Distinct Chromosomal Imbalances in Nonpolypoid and Polypoid Colorectal Adenomas Indicate Different Genetic Pathways in the Development of Colorectal Neoplasms. American Journal of Pathology, 2003, 163, 287-294.	1.9	43
114	Pharmacokinetic and pharmacometabolomic study of pirfenidone in normal mouse tissues using high mass resolution MALDI-FTICR-mass spectrometry imaging. Histochemistry and Cell Biology, 2016, 145, 201-211.	0.8	43
115	In vivo imaging of CT26 mouse tumours by using cmHsp70.1 monoclonal antibody. Journal of Cellular and Molecular Medicine, 2011, 15, 874-887.	1.6	42
116	Optoacoustic Imaging and Staging of Inflammation in a Murine Model of Arthritis. Arthritis and Rheumatology, 2014, 66, 2071-2078.	2.9	42
117	Three-Dimensional Quantitative Co-Mapping of Pulmonary Morphology and Nanoparticle Distribution with Cellular Resolution in Nondissected Murine Lungs. ACS Nano, 2019, 13, 1029-1041.	7.3	42
118	Glutathione peroxidase 4 and vitamin E control reticulocyte maturation, stress erythropoiesis and iron homeostasis. Haematologica, 2020, 105, 937-950.	1.7	42
119	Post-surgical adhesions are triggered by calcium-dependent membrane bridges between mesothelial surfaces. Nature Communications, 2020, 11, 3068.	5.8	42
120	Coamplification and coexpression of GRB7 and ERBB2 is found in high grade intraepithelial neoplasia and in invasive Barrett's carcinoma. International Journal of Cancer, 2004, 112, 747-753.	2.3	41
121	The impact of Cysteine-Rich Intestinal Protein 1 (CRIP1) in human breast cancer. Molecular Cancer, 2013, 12, 28.	7.9	41
122	Assessment of Myocardial Infarction and Postinfarction Scar Remodeling With an Elastin-Specific Magnetic Resonance Agent. Circulation: Cardiovascular Imaging, 2014, 7, 321-329.	1.3	41
123	Novel Approach of MALDI Drug Imaging, Immunohistochemistry, and Digital Image Analysis for Drug Distribution Studies in Tissues. Analytical Chemistry, 2014, 86, 10568-10575.	3.2	41
124	CLIP2 as radiation biomarker in papillary thyroid carcinoma. Oncogene, 2015, 34, 3917-3925.	2.6	41
125	Highâ€resolution metabolite imaging of light and dark treated retina using <scp>MALDI</scp> â€ <scp>FTICR</scp> mass spectrometry. Proteomics, 2014, 14, 913-923.	1.3	40
126	MSiMass List: A Public Database of Identifications for Protein MALDI MS Imaging. Journal of Proteome Research, 2014, 13, 1138-1142.	1.8	40

#	Article	IF	CITATIONS
127	Characterization of Magnetic Viral Complexes for Targeted Delivery in Oncology. Theranostics, 2015, 5, 667-685.	4.6	40
128	Genome-wide analysis of genetic alterations in Barrett's adenocarcinoma using single nucleotide polymorphism arrays. Laboratory Investigation, 2009, 89, 385-397.	1.7	39
129	Round robin study of formalin-fixed paraffin-embedded tissues in mass spectrometry imaging. Analytical and Bioanalytical Chemistry, 2018, 410, 5969-5980.	1.9	39
130	Active steroid hormone synthesis renders adrenocortical cells highly susceptible to type II ferroptosis induction. Cell Death and Disease, 2020, 11, 192.	2.7	39
131	Analysis of thePTCH coding region in human rhabdomyosarcoma. Human Mutation, 2002, 20, 233-234.	1.1	38
132	Human archival tissues provide a valuable source for the analysis of spatial genome organization. Histochemistry and Cell Biology, 2005, 123, 229-238.	0.8	38
133	Classification of mass-spectrometric data in clinical proteomics using learning vector quantization methods. Briefings in Bioinformatics, 2007, 9, 129-143.	3.2	38
134	Farnesoid X receptor protects human and murine gastric epithelial cells against inflammation-induced damage. Biochemical Journal, 2011, 438, 315-323.	1.7	38
135	Signalling networks associated with urokinaseâ€type plasminogen activator (uPA) and its inhibitor PAlâ€1 in breast cancer tissues: new insights from protein microarray analysis. Journal of Pathology, 2011, 223, 54-63.	2.1	38
136	Copy number gains on 22q13 in adenoid cystic carcinoma of the salivary gland revealed by comparative genomic hybridization and tissue microarray analysis. Cancer Genetics and Cytogenetics, 2005, 159, 89-95.	1.0	37
137	FLT-PET Is Superior to FDG-PET for Very Early Response Prediction in NPM-ALK-Positive Lymphoma Treated with Targeted Therapy. Cancer Research, 2012, 72, 5014-5024.	0.4	37
138	Knocking Down of Isoprene Emission Modifies the Lipid Matrix of Thylakoid Membranes and Influences the Chloroplast Ultrastructure in Poplar. Plant Physiology, 2015, 168, 859-870.	2.3	37
139	High-Resolution Tissue Mass Spectrometry Imaging Reveals a Refined Functional Anatomy of the Human Adult Adrenal Gland. Endocrinology, 2018, 159, 1511-1524.	1.4	37
140	Distinct cytogenetic alterations in squamous intraepithelial lesions of the cervix revealed by laser-assisted microdissection and comparative genomic hybridization. , 1998, 84, 375-379.		36
141	Stromal cell-associated expression of kallikrein-related peptidase 6 (KLK6) indicates poor prognosis of ovarian cancer patients. Biological Chemistry, 2012, 393, 391-401.	1.2	36
142	Epstein–Barr Virus in Gastro-Esophageal Adenocarcinomas – Single Center Experiences in the Context of Current Literature. Frontiers in Oncology, 2015, 5, 73.	1.3	36
143	Chromosomal Imbalances are Associated with Metastasis-Free Survival in Breast Cancer Patients. Analytical Cellular Pathology, 2002, 24, 77-87.	2.1	35
144	Efficient internalization and intracellular translocation of inhaled gold nanoparticles in rat alveolar macrophages. Nanomedicine, 2012, 7, 855-865.	1.7	35

#	Article	IF	CITATIONS
145	Bezafibrate Improves Insulin Sensitivity and Metabolic Flexibility in STZ-Induced Diabetic Mice. Diabetes, 2016, 65, 2540-2552.	0.3	35
146	Elemental bioimaging and speciation analysis for the investigation of Wilson's disease using μXRF and XANES. Metallomics, 2016, 8, 648-653.	1.0	35
147	Correlative mass spectrometry imaging, applying timeâ€ofâ€flight secondary ion mass spectrometry and atmospheric pressure matrixâ€assisted laser desorption/ionization to a single tissue section. Rapid Communications in Mass Spectrometry, 2018, 32, 159-166.	0.7	35
148	Epidermal growth factor receptor (EGFR) is an independent adverse prognostic factor in esophageal adenocarcinoma patients treated with cisplatin-based neoadjuvant chemotherapy. Oncotarget, 2014, 5, 6620-6632.	0.8	35
149	RET rearrangements in post-Chernobyl papillary thyroid carcinomas with a short latency analysed by interphase FISH. British Journal of Cancer, 2006, 94, 1472-1477.	2.9	34
150	Array CGH demonstrates characteristic aberration signatures in human papillary thyroid carcinomas governed by RET/PTC. Oncogene, 2008, 27, 4592-4602.	2.6	34
151	High fat diet-induced modifications in membrane lipid and mitochondrial-membrane protein signatures precede the development of hepatic insulin resistance in mice. Molecular Metabolism, 2015, 4, 39-50.	3.0	34
152	Threshold Analysis and Biodistribution of Fluorescently Labeled Bevacizumab in Human Breast Cancer. Cancer Research, 2017, 77, 623-631.	0.4	34
153	Native glycan fragments detected by MALDI-FT-ICR mass spectrometry imaging impact gastric cancer biology and patient outcome. Oncotarget, 2017, 8, 68012-68025.	0.8	34
154	Facile Synthesis of a Croconaineâ€Based Nanoformulation for Optoacoustic Imaging and Photothermal Therapy. Advanced Healthcare Materials, 2021, 10, e2002115.	3.9	34
155	The molecular pathology of Barrett's esophagus. Histology and Histopathology, 1999, 14, 553-9.	0.5	34
156	Molecular Genetic Changes in Metastatic Primary Barrett's Adenocarcinoma and Related Lymph Node Metastases: Comparison with Nonmetastatic Barrett's Adenocarcinoma. Modern Pathology, 2000, 13, 814-824.	2.9	33
157	Heterogeneous Chromosomal Aberrations in Intraductal Breast Lesions Adjacent to Invasive Carcinoma. Analytical Cellular Pathology, 2000, 20, 17-24.	2.1	33
158	Chromosomal changes characterize head and neck cancer with poor prognosis. Journal of Molecular Medicine, 2008, 86, 1353-1365.	1.7	33
159	Novel gene rearrangements in transformed breast cells identified by high-resolution breakpoint analysis of chromosomal aberrations. Endocrine-Related Cancer, 2010, 17, 87-98.	1.6	33
160	Diet intervention reduces uptake of αvβ3 integrin-targeted PET tracer 18F-galacto-RGD in mouse atherosclerotic plaques. Journal of Nuclear Cardiology, 2012, 19, 775-784.	1.4	33
161	Iron-Sequestering Nanocompartments as Multiplexed Electron Microscopy Gene Reporters. ACS Nano, 2019, 13, 8114-8123.	7.3	33
162	Mass Spectrometry Imaging Establishes 2 Distinct Metabolic Phenotypes of Aldosterone-Producing Cell Clusters in Primary Aldosteronism. Hypertension, 2020, 75, 634-644.	1.3	33

#	Article	IF	CITATIONS
163	Histopathological diagnosis of Barrett's mucosa and associated neoplasias: results of a consensus conference of the Working Group for Gastroenterological Pathology of the German Society for Pathology on 22 September 2001 in Erlangen. Virchows Archiv Fur Pathologische Anatomie Und Physiologie Und Fur Klinische Medizin, 2003, 443, 597-601.	1.4	32
164	Numerical and structural centrosome aberrations are an early and stable event in the adenoma–carcinoma sequence of colorectal carcinomas. Virchows Archiv Fur Pathologische Anatomie Und Physiologie Und Fur Klinische Medizin, 2005, 447, 61-65.	1.4	32
165	Filtering blue light reduces lightâ€induced oxidative stress, senescence and accumulation of extracellular matrix proteins in human retinal pigment epithelium cells. Clinical and Experimental Ophthalmology, 2012, 40, e87-97.	1.3	32
166	De novo discovery of metabolic heterogeneity with immunophenotype-guided imaging mass spectrometry. Molecular Metabolism, 2020, 36, 100953.	3.0	32
167	Microarray comparative genomic hybridization analysis of tubular breast carcinoma shows recurrent loss of the CDH13 locus on 16q. Human Pathology, 2008, 39, 1621-1629.	1.1	31
168	Element bioimaging of liver needle biopsy specimens from patients with Wilson's disease by laser ablation-inductively coupled plasma-mass spectrometry. Journal of Trace Elements in Medicine and Biology, 2016, 35, 97-102.	1.5	31
169	Comparison of loss of heterozygosity and microsatellite instability in adenocarcinomas of the distal esophagus and proximal stomach. Virchows Archiv Fur Pathologische Anatomie Und Physiologie Und Fur Klinische Medizin, 2000, 437, 605-610.	1.4	30
170	Interaction of Snail and p38 mitogen-activated protein kinase results in shorter overall survival of ovarian cancer patients. Virchows Archiv Fur Pathologische Anatomie Und Physiologie Und Fur Klinische Medizin, 2010, 457, 705-713.	1.4	30
171	Epidermal growth factor receptor, phosphatidylinositol-3-kinase catalytic subunit/PTEN, and KRAS/NRAS/BRAF in primary resected esophageal adenocarcinomas: loss of PTEN is associated with worse clinical outcome. Human Pathology, 2013, 44, 829-836.	1.1	30
172	Centrosome-, chromosomal-passenger- and cell-cycle-associated mRNAs are differentially regulated in the development of sporadic colorectal cancer. Journal of Pathology, 2006, 208, 462-472.	2.1	29
173	Activation of epidermal growth factor receptor results in Snail protein but not mRNA overexpression in endometrial cancer. Journal of Cellular and Molecular Medicine, 2009, 13, 3858-3867.	1.6	29
174	uPA and PAI-1-Related Signaling Pathways Differ between Primary Breast Cancers and Lymph Node Metastases. Translational Oncology, 2012, 5, 98-IN3.	1.7	29
175	Spatial Autocorrelation in Mass Spectrometry Imaging. Analytical Chemistry, 2016, 88, 5871-5878.	3.2	29
176	Expression of mi <scp>RNA</scp> â€26bâ€5p and its target <scp>TRPS</scp> 1 is associated with radiation exposure in postâ€ <scp>C</scp> hernobyl breast cancer. International Journal of Cancer, 2018, 142, 573-583.	2.3	29
177	Chronic d-serine supplementation impairs insulin secretion. Molecular Metabolism, 2018, 16, 191-202.	3.0	29
178	Immunotherapeutic Targeting of Membrane Hsp70-Expressing Tumors Using Recombinant Human Granzyme B. PLoS ONE, 2012, 7, e41341.	1.1	29
179	CRIP1 expression is correlated with a favorable outcome and less metastases in osteosarcoma patients. Oncotarget, 2011, 2, 970-975.	0.8	29
180	Evaluation of C-ErbB-2 Overexpression and Her-2/ <i>neu</i> Gene Copy Number Heterogeneity in Barrett's Adenocarcinoma. Analytical Cellular Pathology, 2000, 20, 25-32.	2.1	28

#	Article	IF	CITATIONS
181	Hematopoietically expressed homeobox is a target gene of farnesoid X receptor in chenodeoxycholic acid-induced liver hypertrophy. Hepatology, 2009, 49, 979-988.	3.6	28
182	Super-resolution segmentation of imaging mass spectrometry data: Solving the issue of low lateral resolution. Journal of Proteomics, 2011, 75, 237-245.	1.2	28
183	Current frontiers in clinical research application of MALDI imaging mass spectrometry. Expert Review of Proteomics, 2013, 10, 259-273.	1.3	28
184	In Situ Metabolomics in Cancer by Mass Spectrometry Imaging. Advances in Cancer Research, 2017, 134, 117-132.	1.9	28
185	hIAPP forms toxic oligomers in plasma. Chemical Communications, 2018, 54, 5426-5429.	2.2	28
186	Definitive chemoradiotherapy in patients with squamous cell cancers of the head and neck - results from an unselected cohort of the clinical cooperation group "Personalized Radiotherapy in Head and Neck Cancer― Radiation Oncology, 2020, 15, 7.	1.2	28
187	X-Ray Phase-Contrast CT of a Pancreatic Ductal Adenocarcinoma Mouse Model. PLoS ONE, 2013, 8, e58439.	1.1	28
188	Modeling Therapy Response and Spatial Tissue Distribution of Erlotinib in Pancreatic Cancer. Molecular Cancer Therapeutics, 2016, 15, 1145-1152.	1.9	27
189	In situ metabolomics of aldosterone-producing adenomas. JCI Insight, 2019, 4, .	2.3	27
190	Spatial Metabolomics Identifies Distinct Tumor-Specific Subtypes in Gastric Cancer Patients. Clinical Cancer Research, 2022, 28, 2865-2877.	3.2	27
191	Developmental expression of neuromodulators in the central complex of the grasshopper <i>Schistocerca gregaria</i> . Journal of Morphology, 2010, 271, 1509-1526.	0.6	26
192	High-resolution MALDI mass spectrometric imaging of lipids in the mammalian retina. Histochemistry and Cell Biology, 2015, 143, 453-462.	0.8	26
193	uPAR enhances malignant potential of triple-negative breast cancer by directly interacting with uPA and IGF1R. BMC Cancer, 2016, 16, 615.	1.1	26
194	Pharmacometabolic response to pirfenidone in pulmonary fibrosis detected by MALDI-FTICR-MSI. European Respiratory Journal, 2018, 52, 1702314.	3.1	26
195	Evidence of Prognostic Relevant Expression Profiles of Heat-Shock Proteins and Glucose-Regulated Proteins in Oesophageal Adenocarcinomas. PLoS ONE, 2012, 7, e41420.	1.1	25
196	Model Matters: Differences in Orthotopic Rat Hepatocellular Carcinoma Physiology Determine Therapy Response to Sorafenib. Clinical Cancer Research, 2015, 21, 4440-4450.	3.2	25
197	Platelet GPIIb supports initial pulmonary retention but inhibits subsequent proliferation of melanoma cells during hematogenic metastasis. PLoS ONE, 2017, 12, e0172788.	1.1	25
198	Molecular similarities and differences from human pulmonary fibrosis and corresponding mouse model: MALDI imaging mass spectrometry in comparative medicine. Laboratory Investigation, 2018, 98, 141-149.	1.7	25

#	Article	IF	CITATIONS
199	Association between HSP90 and Her2 in Gastric and Gastroesophageal Carcinomas. PLoS ONE, 2013, 8, e69098.	1.1	25
200	Premature Apoptosis of <i>Chlamydia</i> â€Infected Cells Disrupts Chlamydial Development. Journal of Infectious Diseases, 2008, 198, 1536-1544.	1.9	24
201	Direct Molecular Tissue Analysis by MALDI Imaging Mass Spectrometry in the Field of Gastrointestinal Disease. Gastroenterology, 2012, 143, 544-549.e2.	0.6	24
202	Spatially Resolved Quantification of Gadolinium(III)â€Based Magnetic Resonance Agents in Tissue by MALDI Imaging Mass Spectrometry after In Vivo MRI. Angewandte Chemie - International Edition, 2015, 54, 4279-4283.	7.2	24
203	How Suitable is Matrix-Assisted Laser Desorption/Ionization-Time-of-Flight for Metabolite Imaging from Clinical Formalin-Fixed and Paraffin-Embedded Tissue Samples in Comparison to Matrix-Assisted Laser Desorption/Ionization-Fourier Transform Ion Cyclotron Resonance Mass Spectrometry?. Analytical Chemistry, 2016, 88, 5281-5289.	3.2	24
204	Postoperative (chemo) radiation in patients with squamous cell cancers of the head and neck – clinical results from the cohort of the clinical cooperation group "Personalized Radiotherapy in Head and Neck Cancer― Radiation Oncology, 2018, 13, 123.	1.2	24
205	Impact of Extrinsic and Intrinsic Hypoxia on Catecholamine Biosynthesis in Absence or Presence of Hif2α in Pheochromocytoma Cells. Cancers, 2019, 11, 594.	1.7	24
206	MALDI mass spectrometry imaging of formalin-fixed paraffin-embedded tissues in clinical research. Histology and Histopathology, 2014, 29, 1365-76.	0.5	24
207	Adrenal tropism of SARS-CoV-2 and adrenal findings in a post-mortem case series of patients with severe fatal COVID-19. Nature Communications, 2022, 13, 1589.	5.8	24
208	High-Resolution Multispectral Optoacoustic Tomography of the Vascularization and Constitutive Hypoxemia of Cancerous Tumors. Neoplasia, 2016, 18, 459-467.	2.3	23
209	Protein Microarray-based Comparison of HER2, Estrogen Receptor, and Progesterone Receptor Status in Core Biopsies and Surgical Specimens From FFPE Breast Cancer Tissues. Applied Immunohistochemistry and Molecular Morphology, 2011, 19, 300-305.	0.6	22
210	<i>In situ</i> drug and metabolite analysis in biological and clinical research by MALDIÂMS imaging. Bioanalysis, 2014, 6, 1241-1253.	0.6	22
211	Light sheet fluorescence microscopy guided MALDI-imaging mass spectrometry of cleared tissue samples. Scientific Reports, 2020, 10, 14461.	1.6	22
212	Profiling signalling pathways in formalinâ€fixed and paraffinâ€embedded breast cancer tissues reveals crossâ€ŧalk between EGFR, HER2, HER3 and uPAR. Journal of Cellular Physiology, 2012, 227, 204-212.	2.0	21
213	Cardioprotective C-kit+ Bone Marrow Cells Attenuate Apoptosis after Acute Myocardial Infarction in Mice - In-vivo Assessment with Fluorescence Molecular Imaging. Theranostics, 2013, 3, 903-913.	4.6	21
214	A prognostic mRNA expression signature of four 16q24.3 genes in radio(chemo)therapyâ€ŧreated head and neck squamous cell carcinoma (HNSCC). Molecular Oncology, 2018, 12, 2085-2101.	2.1	21
215	Multimodal Precision Imaging of Pulmonary Nanoparticle Delivery in Mice: Dynamics of Application, Spatial Distribution, and Dosimetry. Small, 2019, 15, e1904112.	5.2	21
216	Giant ancient schwannoma of pancreatic head treated by extended pancreatoduodenectomy. Pancreatology, 2004, 4, 505-508.	0.5	20

#	Article	IF	CITATIONS
217	MALDI Imaging Mass Spectrometry for Direct Tissue Analysis. Methods in Molecular Biology, 2012, 931, 537-546.	0.4	20
218	Expression patterns of programmed death-ligand 1 in esophageal adenocarcinomas: comparison between primary tumors and metastases. Cancer Immunology, Immunotherapy, 2017, 66, 777-786.	2.0	20
219	Derangements of amino acids in cachectic skeletal muscle are caused by mitochondrial dysfunction. Journal of Cachexia, Sarcopenia and Muscle, 2020, 11, 226-240.	2.9	20
220	Proteomic and metabolic prediction of response to therapy in gastric cancer. World Journal of Gastroenterology, 2014, 20, 13648.	1.4	20
221	Digital pathology: Multiple instance learning can detect Barrett's cancer. , 2014, , .		19
222	Clinical Significance of NOTCH1 and NOTCH2 Expression in Gastric Carcinomas: An Immunohistochemical Study. Frontiers in Oncology, 2015, 5, 94.	1.3	19
223	RNAi-mediated downregulation of poplar plasma membrane intrinsic proteins (PIPs) changes plasma membrane proteome composition and affects leaf physiology. Journal of Proteomics, 2015, 128, 321-332.	1.2	19
224	In situ detection of histone variants and modifications in mouse brain using imaging mass spectrometry. Proteomics, 2016, 16, 437-447.	1.3	19
225	Prognostic Relevance of Steroid Sulfation in Adrenocortical Carcinoma Revealed by Molecular Phenotyping Using High-Resolution Mass Spectrometry Imaging. Clinical Chemistry, 2019, 65, 1276-1286.	1.5	19
226	Croconaine-based nanoparticles enable efficient optoacoustic imaging of murine brain tumors. Photoacoustics, 2021, 22, 100263.	4.4	19
227	Sphingomyelin Synthase 1 Is Essential for Male Fertility in Mice. PLoS ONE, 2016, 11, e0164298.	1.1	19
228	Spatial metabolomics for evaluating response to neoadjuvant therapy in nonâ€small cell lung cancer patients. Cancer Communications, 2022, 42, 517-535.	3.7	19
229	Proteomic and metabolic prediction of response to therapy in gastrointestinal cancers. Nature Reviews Gastroenterology and Hepatology, 2009, 6, 170-183.	8.2	18
230	Isolation of Highly Pure Rat Liver Mitochondria with the Aid of Zone-Electrophoresis in a Free Flow Device (ZE-FFE). Methods in Molecular Biology, 2008, 424, 333-348.	0.4	18
231	Microdissection of Tissue Sections: Application to the Molecular Genetic Characterisation of Premalignant Lesions. Pathobiology, 2000, 68, 9-17.	1.9	17
232	Inhibition of MMP-dependent chemotaxis and amelioration of experimental autoimmune uveitis with a selective metalloproteinase-2 and -9 inhibitor. Journal of Neuroimmunology, 2004, 155, 13-20.	1.1	17
233	MTO1-Deficient Mouse Model Mirrors the Human Phenotype Showing Complex I Defect and Cardiomyopathy. PLoS ONE, 2014, 9, e114918.	1.1	17
234	A rapid ex vivo tissue model for optimising drug detection and ionisation in MALDI imaging studies. Histochemistry and Cell Biology, 2014, 142, 361-371.	0.8	17

#	Article	IF	CITATIONS
235	Integrin-Targeted Hybrid Fluorescence Molecular Tomography/X-ray Computed Tomography for Imaging Tumor Progression and Early Response in Non-Small Cell Lung Cancer. Neoplasia, 2017, 19, 8-16.	2.3	17
236	Tissue kallikrein-related peptidase 4 (KLK4), a novel biomarker in triple-negative breast cancer. Biological Chemistry, 2017, 398, 1151-1164.	1.2	17
237	Precise measurement of the E-cadherin repressor Snail in formalin-fixed endometrial carcinoma using protein lysate microarrays. Clinical and Experimental Metastasis, 2008, 25, 679-683.	1.7	16
238	Translatomic profiling reveals novel self-restricting virus-host interactions during HBV infection. Journal of Hepatology, 2021, 75, 74-85.	1.8	16
239	Sequential Multilocus Fluorescence In Situ Hybridization Can Detect Complex Patterns of Increased Gene Dosage at the Single Cell Level in Tissue Sections. Laboratory Investigation, 2001, 81, 1457-1459.	1.7	15
240	Nuclear Position and Shape Deformation of Chromosome 8 Territories in Pancreatic Ductal Adenocarcinoma. Analytical Cellular Pathology, 2011, 34, 21-33.	0.7	15
241	Tumor Uptake of Anti-CD20 Fabs Depends on Tumor Perfusion. Journal of Nuclear Medicine, 2016, 57, 1971-1977.	2.8	15
242	PITX2 DNA-methylation predicts response to anthracycline-based adjuvant chemotherapy in triple-negative breast cancer patients. International Journal of Oncology, 2018, 52, 755-767.	1.4	15
243	Optimized protocol for metabolomic and lipidomic profiling in formalin-fixed paraffin-embedded kidney tissue by LC-MS. Analytica Chimica Acta, 2020, 1134, 125-135.	2.6	15
244	Enhanced efficacy of combined 213Bi-DTPA-F3 and paclitaxel therapy of peritoneal carcinomatosis is mediated by enhanced induction of apoptosis and G2/M phase arrest. European Journal of Nuclear Medicine and Molecular Imaging, 2012, 39, 1886-1897.	3.3	14
245	Optical mesoscopy without the scatter: broadband multispectral optoacoustic mesoscopy. Biomedical Optics Express, 2015, 6, 3134.	1.5	14
246	PAXgene fixation enables comprehensive metabolomic and proteomic analyses of tissue specimens by MALDI MSI. Biochimica Et Biophysica Acta - General Subjects, 2018, 1862, 51-60.	1.1	14
247	Heat Shock Protein 90 as a Prognostic Marker and Therapeutic Target for Adrenocortical Carcinoma. Frontiers in Endocrinology, 2019, 10, 487.	1.5	14
248	Inhibition of metabotropic glutamate receptor III facilitates sensitization to alkylating chemotherapeutics in glioblastoma. Cell Death and Disease, 2021, 12, 723.	2.7	14
249	Identification and characterization of distinct brown adipocyte subtypes in C57BL/6J mice. Life Science Alliance, 2021, 4, e202000924.	1.3	14
250	Heat Shock Protein 90 (HSP90) and Her2 in Adenocarcinomas of the Esophagus. Cancers, 2014, 6, 1382-1393.	1.7	13
251	MALDI imaging mass spectrometry as a novel tool for detecting histone modifications in clinical tissue samples. Expert Review of Proteomics, 2016, 13, 275-284.	1.3	13
252	Plasmin(ogen) serves as a favorable biomarker for prediction of survival in advanced high-grade serous ovarian cancer. Biological Chemistry, 2017, 398, 765-773.	1.2	13

#	Article	IF	CITATIONS
253	Investigating the influence of standard staining procedures on the copper distribution and concentration in Wilson's disease liver samples by laser ablation-inductively coupled plasma-mass spectrometry. Journal of Trace Elements in Medicine and Biology, 2017, 44, 71-75.	1.5	13
254	Therapy-Related Transcriptional Subtypes in Matched Primary and Recurrent Head and Neck Cancer. Clinical Cancer Research, 2022, 28, 1038-1052.	3.2	13
255	Centrosome abnormalities in head and neck squamous cell carcinoma (HNSCC). Acta Oto-Laryngologica, 2009, 129, 205-213.	0.3	12
256	Supremacy of modern morphometry in typing renal oncocytoma and malignant look-alikes. Histochemistry and Cell Biology, 2015, 144, 147-156.	0.8	12
257	Molecular imaging of myocardial infarction with Gadofluorine P – A combined magnetic resonance and mass spectrometry imaging approach. Heliyon, 2018, 4, e00606.	1.4	12
258	Beam size limit for pencil minibeam radiotherapy determined from side effects in an in-vivo mouse ear model. PLoS ONE, 2019, 14, e0221454.	1.1	12
259	Inhibition of HSP90 as a Strategy to Radiosensitize Glioblastoma: Targeting the DNA Damage Response and Beyond. Frontiers in Oncology, 2021, 11, 612354.	1.3	12
260	Mass spectrometry imaging identifies metabolic patterns associated with malignant potential in pheochromocytoma and paraganglioma. European Journal of Endocrinology, 2021, 185, 179-191.	1.9	12
261	Nuclear position and shape deformation of chromosome 8 territories in pancreatic ductal adenocarcinoma. Analytical Cellular Pathology, 2011, 34, 21-33.	0.7	12
262	Patterns of Carbon-Bound Exogenous Compounds in Patients with Lung Cancer and Association with Disease Pathophysiology. Cancer Research, 2021, 81, 5862-5875.	0.4	12
263	Establishment and Molecular Cytogenetic Characterization of a Cell Culture Model of Head and Neck Squamous Cell Carcinoma (HNSCC). Genes, 2010, 1, 388-412.	1.0	11
264	Positron emission tomographic monitoring of dual phosphatidylinositol-3-kinase and mTOR inhibition in anaplastic large cell lymphoma. OncoTargets and Therapy, 2014, 7, 789.	1.0	11
265	Metabolic tumor constitution is superior to tumor regression grading for evaluating response to neoadjuvant therapy of esophageal adenocarcinoma patients. Journal of Pathology, 2022, 256, 202-213.	2.1	11
266	Bile Acids Down-Regulate Caveolin-1 in Esophageal Epithelial Cells through Sterol Responsive Element-Binding Protein. Molecular Endocrinology, 2012, 26, 819-832.	3.7	10
267	Early recognition of lung cancer by integrin targeted imaging in <scp>K</scp> â€ras mouse model. International Journal of Cancer, 2015, 137, 1107-1118.	2.3	10
268	A genomic copy number signature predicts radiation exposure in post―C hernobyl breast cancer. International Journal of Cancer, 2018, 143, 1505-1515.	2.3	10
269	Multimodal analysis of formalin-fixed and paraffin-embedded tissue by MALDI imaging and fluorescence in situ hybridization for combined genetic and metabolic analysis. Laboratory Investigation, 2019, 99, 1535-1546.	1.7	10
270	Novel methods in adrenal research: a metabolomics approach. Histochemistry and Cell Biology, 2019, 151, 201-216.	0.8	10

#	Article	IF	CITATIONS
271	Molecular imaging for early prediction of response to Sorafenib treatment in sarcoma. American Journal of Nuclear Medicine and Molecular Imaging, 2013, 4, 70-9.	1.0	10
272	Heterotopic Pancreatitis with Obstruction of the Major Duodenal Papilla - A Rare Trigger of Obstructive Orthotopic Pancreatitis. Pancreatology, 2004, 4, 244-248.	0.5	9
273	Detection of Lymph Node Involvement by Cytokeratin Immunohistochemistry is an Independent Prognostic Factor After Curative Resection of Esophageal Cancer. Journal of Gastrointestinal Surgery, 2011, 15, 29-37.	0.9	9
274	A new model system identifies epidermal growth factor receptor-human epidermal growth factor receptor 2 (HER2) and HER2-human epidermal growth factor receptor 3 heterodimers as potent inducers of oesophageal epithelial cell invasion. Journal of Pathology, 2017, 243, 481-495.	2.1	9
275	Mass Spectrometry Imaging of atherosclerosis-affine Gadofluorine following Magnetic Resonance Imaging. Scientific Reports, 2020, 10, 79.	1.6	9
276	A practical guide to unbiased quantitative morphological analyses of the gills of rainbow trout (Oncorhynchus mykiss) in ecotoxicological studies. PLoS ONE, 2020, 15, e0243462.	1.1	9
277	Extensive ductal carcinoma In situ with small foci of invasive ductal carcinoma: Evidence of genetic resemblance by CGH. International Journal of Cancer, 2000, 85, 82.	2.3	9
278	Multiomics interrogation into HBV (Hepatitis B virus)-host interaction reveals novel coding potential in human genome, and identifies canonical and non-canonical proteins as host restriction factors against HBV. Cell Discovery, 2021, 7, 105.	3.1	9
279	Integrative Clustering in Mass Spectrometry Imaging for Enhanced Patient Stratification. Proteomics - Clinical Applications, 2019, 13, e1800137.	0.8	8
280	MALDI Mass Spectrometry Imaging—Prognostic Pathways and Metabolites for Renal Cell Carcinomas. Cancers, 2022, 14, 1763.	1.7	8
281	In Brief: The (molecular) pathogenesis of Barrett's oesophagus. Journal of Pathology, 2014, 232, 383-385.	2.1	7
282	Early detection of radiation-induced lung damage with X-ray dark-field radiography in mice. European Radiology, 2021, 31, 4175-4183.	2.3	7
283	Cyr61 and YB-1 are novel interacting partners of uPAR and elevate the malignancy of triple-negative breast cancer. Oncotarget, 2016, 7, 44062-44075.	0.8	7
284	The synergism of spatial metabolomics and morphometry improves machine learningâ€based renal tumour subtype classification. Clinical and Translational Medicine, 2022, 12, e666.	1.7	7
285	A Case of Heterogeneous Breast Cancer with Clonally Expanded T-Cells in the HER2+ and Metastasis of the HER2â^' Tumor Cells. Breast Journal, 2008, 14, 487-491.	0.4	6
286	In situ metabolomics in cancer tissue by high-resolution mass spectrometry imaging. , 2019, , 253-279.		6
287	Digital scoring of EpCAM and slug expression as prognostic markers in head and neck squamous cell carcinomas. Molecular Oncology, 2021, 15, 1040-1053.	2.1	6
288	In Situ Metabolomics Expands the Spectrum of Renal Tumours Positive on 99mTc-sestamibi Single Photon Emission Computed Tomography/Computed Tomography Examination. European Urology Open Science, 2020, 22, 88-96.	0.2	6

#	Article	IF	CITATIONS
289	Dusp8 affects hippocampal size and behavior in mice and humans. Scientific Reports, 2019, 9, 19483.	1.6	5
290	Effect of Dietary Sodium Modulation on Pig Adrenal Steroidogenesis and Transcriptome Profiles. Hypertension, 2020, 76, 1769-1777.	1.3	5
291	Assessment of kallikrein-related peptidase 5 (KLK5) protein expression in tumor tissue of advanced ovarian cancer patients by immunohistochemistry and ELISA: correlation with clinical outcome. American Journal of Cancer Research, 2016, 6, 61-70.	1.4	5
292	Metabolomic therapy response prediction in pretherapeutic tissue biopsies for trastuzumab in patients with HER2â€positive advanced gastric cancer. Clinical and Translational Medicine, 2021, 11, e547.	1.7	4
293	Combining gene expression analysis of gastric cancer cell lines and tumor specimens to identify biomarkers for anti-HER therapies—the role of HAS2, SHB and HBEGF. BMC Cancer, 2022, 22, 254.	1.1	4
294	In situ Metabolite Mass Spectrometry Imaging: New Insights into the Adrenal Gland. Hormone and Metabolic Research, 2020, 52, 435-447.	0.7	3
295	Functional imaging in combination with mutation status aids prediction of response to inhibiting B-cell receptor signaling in lymphoma. Oncotarget, 2017, 8, 78917-78929.	0.8	3
296	PITX2 DNA-Methylation: Predictive versus Prognostic Value for Anthracycline-Based Chemotherapy in Triple-Negative Breast Cancer Patients. Breast Care, 2021, 16, 523-531.	0.8	3
297	Native glycan fragments detected by MALDI mass spectrometry imaging are independent prognostic factors in pancreatic ductal adenocarcinoma. EJNMMI Research, 2021, 11, 120.	1.1	3
298	A simple preparation step to remove excess liquid lipids in white adipose tissue enabling improved detection of metabolites via MALDI-FTICR imaging MS. Histochemistry and Cell Biology, 2022, , 1.	0.8	3
299	Re: Clonal Expansion and Loss of Heterozygosity at Chromosomes 9p and 17p in Premalignant Esophageal (Barrett's) Tissue. Journal of the National Cancer Institute, 2000, 92, 1182-1182.	3.0	2
300	A multi-test strategy for adrenal tumours. Lancet Diabetes and Endocrinology,the, 2020, 8, 733-734.	5.5	1
301	Unbiased analysis of obesity related, fat depot specific changes of adipocyte volumes and numbers using light sheet fluorescence microscopy. PLoS ONE, 2021, 16, e0248594.	1.1	1
302	uPA receptor and its interaction partners: Impact as potential therapeutic targets in triple-negative breast cancer Journal of Clinical Oncology, 2015, 33, 150-150.	0.8	1
303	Preclinical Evaluation of CD40-Directed Immunotherapy in B-Cell Lymphoma Using [ <sup>18</sup> F]Fluorothymidine-PET. Advances in Molecular Imaging, 2015, 05, 17-28.	0.3	1
304	Inside front cover: In situ detection of histone variants and modifications in mouse brain using imaging mass spectrometry. Proteomics, 2016, 16, NA.	1.3	0
305	Transcriptomic landscape of radiation-induced murine thyroid proliferative lesions. Endocrine-Related Cancer, 2021, 28, 213-224.	1.6	0

Methods in Cellular and Molecular Pathology. , 2010, , 1-44.

#	Article	IF	CITATIONS
307	MALDI Imaging Mass Spectrometry on Formalin-Fixed Paraffin-Embedded Tissues. , 2011, , 293-295.		0
308	Automated Co-Analysis of MALDI and H&E Images of Retinal Tissue for an Improved Spatial MALDI Resolution. Informatik Aktuell, 2013, , 217-222.	0.4	0
309	LSC Abstract $\hat{a} \in$ " Non-canonical WNT signaling is mediated by extracellular vesicles in pulmonary fibrosis. , 2016, , .		0
310	LSC Abstract $\hat{a} \in$ " Non-canonical WNT signaling is mediated by extracellular vesicles in pulmonary fibrosis. , 2016, , .		0
311	Nintedanib and pirfenidone inhibit collagen synthesis and maturation at several regulatory levels. , 2016, , .		0
312	Fluorescently labeled bevacizumab in human breast cancer: defining the classification threshold. Proceedings of SPIE, 2017, , .	0.8	0
313	Abstract A068: Metabolic signature in lethal vs. nonlethal prostate cancer. , 2018, , .		0
314	Pharmacometabolic effect of pirfenidone treatment in IPF detected by high resolution MALDI-FTICR imaging. , 2018, , .		0
315	High levels of KLK7 protein expression are related to a favorable prognosis in triple-negative breast cancer patients. American Journal of Cancer Research, 2020, 10, 1785-1792.	1.4	0